

Numerical Modelling of Chamfered Bends and Other Microstrip Junctions of General Shape in MMICS

J. X. Zheng and David C. Chang

MIMICAD Center, University of Colorado, Boulder, CO 80309-425

Abstract

A full-wave analysis based upon a spatial-domain moment method, is obtained for finding two-dimensional current distributions, and hence, the scattering matrix for chamfered bends and other microstrip junctions of general shape in MMICs. The numerical simulation program can provide useful design information as well as physical insights for frequencies way up in the millimeter-wave range.

2. Theory

A full-wave integral equation approach is used to provide some design insights into the higher frequency regime. Using an algorithm called P-mesh model reported earlier [1], we have successfully developed a general-purpose computer program which is capable of analyzing microstrip structures of non-rectangular geometry. The new method basically consists of solving the two-dimensional, vector current distribution on the microstrip surface by a spatial-domain moment method. The integral equation to be solved is

$$\int_{s'} \bar{G}(\bar{r}; \bar{r}') \cdot \bar{J}(\bar{r}') ds' = -\bar{E}_t^i \quad \text{for } \bar{r} \in s \quad (1)$$

where \bar{G} is the dyadic Green function; $\bar{J}(\bar{r}')$ is the current distribution in a planar structure s' ; \bar{E}_t^i is the tangential component of the incident electric field.

Applying the Galerkin method to the integral equation gives

$$-j\omega \int_s ds \int_{s'} ds' \left\{ G_m(\bar{r}; \bar{r}') \bar{J}(\bar{r}) \cdot \bar{J}(\bar{r}') + G_e(\bar{r}; \bar{r}') \rho(\bar{r}) \rho(\bar{r}') \right\} = - \int_s ds \bar{E}_t^i(\bar{r}) \cdot \bar{J}(\bar{r}) \quad (2)$$

where $\rho(\bar{r})$ is the charge distribution; $G_{e,m}$ are the electric and magnetic potentials of point source, respectively. When the observation point and the source point are on the same plane,

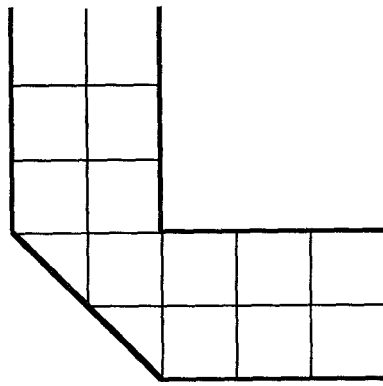


Fig. 1

$$G_m = \frac{\mu_0}{4\pi} \int_0^\infty J_d(\lambda r) \frac{\mu_r \lambda}{\mu_r u_0 + u_n \operatorname{cth} u_n d} d\lambda \quad (3)$$

$$G_e = \frac{1}{4\pi\epsilon_0} \int_0^\infty J_d(\lambda r) \frac{u_0 + \mu_r u_n \operatorname{th} u_n d}{(\epsilon_r u_0 + u_n \operatorname{th} u_n d)(\mu_r u_0 + u_n \operatorname{cth} u_n d)} d\lambda \quad (4)$$

where $u_n = \sqrt{\lambda^2 - \epsilon_r \mu_r}$; $\operatorname{Im}(u_n) \geq 0$ & $\operatorname{Re}(u_n) \geq 0$; r is the distance between the observation point and the source point; d is the substrate thickness; $\epsilon_0 \epsilon_r$ & $\mu_0 \mu_r$ are the permittivity and permeability of the substrate, respectively.

To take advantage of the regularity inherent to the geometry of a given problem, the microstrip structure is divided into a combination of rectangular and triangular cells as shown in Fig.1. A linear approximation is used for the current distribution on each cell, and continuous normal current component between two cells is assumed which, as it turns out, is topologically the same as that of a mesh with branches; hence the name, P(seudo)-mesh. Therefore, the current distribution can be expressed in terms of the branch current of the cells I_n and the multi-face roof-top basis functions $\bar{J}_n(\bar{r})$ as shown in Fig.2

$$\bar{J}(\bar{r}) = \sum_n \bar{J}_n(\bar{r}) I_n \quad (5)$$

Use is made of the Rayleigh Ritz procedure to get the matrix equation

$$[Z_{ij}] [I_j] = [V_i] \quad (6)$$

where

$$Z_{ij} = -j \omega \int_s ds \int_{s'} ds' \left\{ G_m \bar{J}_i(\bar{r}) \cdot \bar{J}_j(\bar{r}') - \omega^2 G_e \nabla_{\bar{r}} \cdot \bar{J}_i \nabla_{\bar{r}'} \cdot \bar{J}_j \right\} \quad (7)$$

$$V_i = - \int_s ds \bar{E}_t^i \cdot \bar{J}_i \quad (8)$$

The potentials $G_{m,e}$ are computed, as in the case of the BCW code developed earlier for the structures of rectangular geometry [5], [6], and curve-fitted into polynomials locally. Therefore, the double surface integrals involved in eq.(7) are of the form

$$Q = \int_{\Delta s} ds \int_{\Delta s'} ds' r^k x^i y^j x^m y^n \quad k = -1, 0, 1, \dots; i, j, m, n = 0 \text{ or } 1 \quad (9)$$

and can be solved analytically when Δs and $\Delta s'$ are any polygons.

The method is well-adapted to cells of different sizes, shapes and orientations.

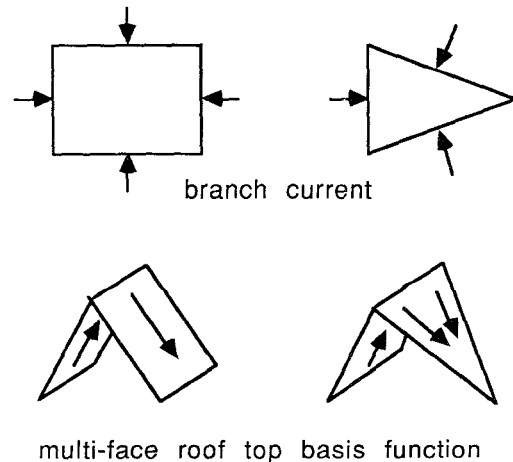


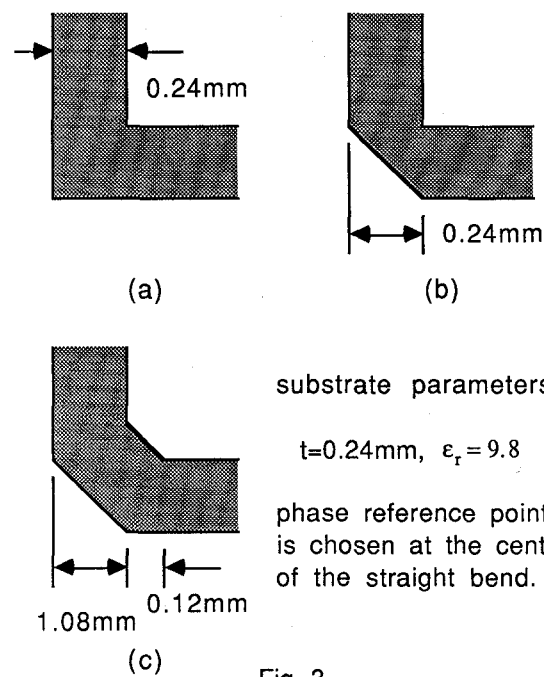
Fig.2

3. Results

The geometry of a right-angle single bend, with and without a chamfered corner, and a right-angle double bend are shown in Fig.3. The scattering matrix for each case is de-embedded from the current distribution obtained from the p-mesh model described in section 2. The program can be run on a HP-300 workstation, or a supercomputer depending upon the number of cells or the desired accuracy for a given problem. To get reasonably accurate values of a scattering matrix, one needs about 20 cells per wavelength in the wave propagation direction, and only one cell in the transverse direction for a typical 50 Ohm line. Generally, a 100 cell problem takes about 30 to 40 minute cpu time on the HP workstation. For illustration, the magnitudes of the x-directed and y-directed current distribution are plotted in Fig.4, for the structure shown in Fig.3a with a voltage source placed away from the junction. It is of interest to note that the current vanishes at the outer corner of the bend but it changes direction round the inner corner.

Figures 5 and 6 show the magnitude and phase, respectively, of S11 and S12 as a function of frequency for the configurations in Fig.3. At the low frequency end, the three structures essentially have the same circuit performance as expected. The differences among the three are indeed noticeable at the high frequency range. It appears that:

- The radiation loss is negligibly small even for frequency as high as 40 GHz for all three types;
- For frequencies beyond 30 GHz, the reflection from the unchamfered corner becomes relatively large;
- Because of the interference between the reflections from the two junctions, a double bend can provide a better overall performance in some frequency range.



substrate parameters:

$$t=0.24\text{mm}, \epsilon_r=9.8$$

phase reference point
is chosen at the center
of the straight bend.

Fig. 3

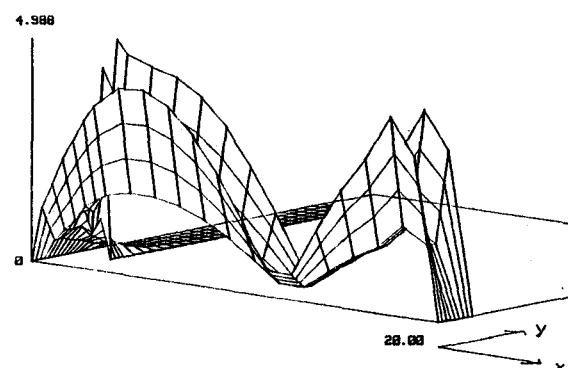


Fig.4 (a) x - directed current.

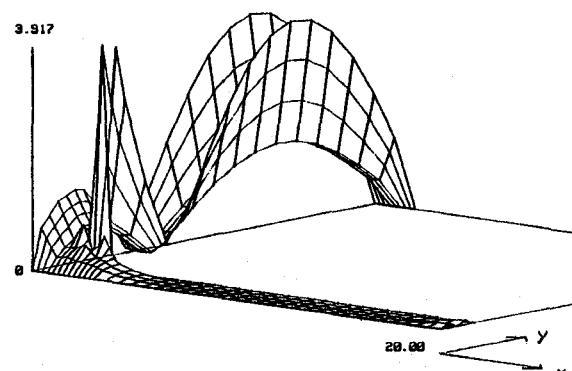


Fig.4 (b) y - directed current.

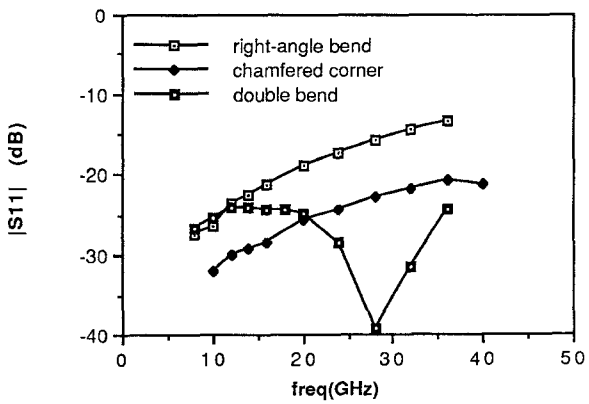


Fig. 5

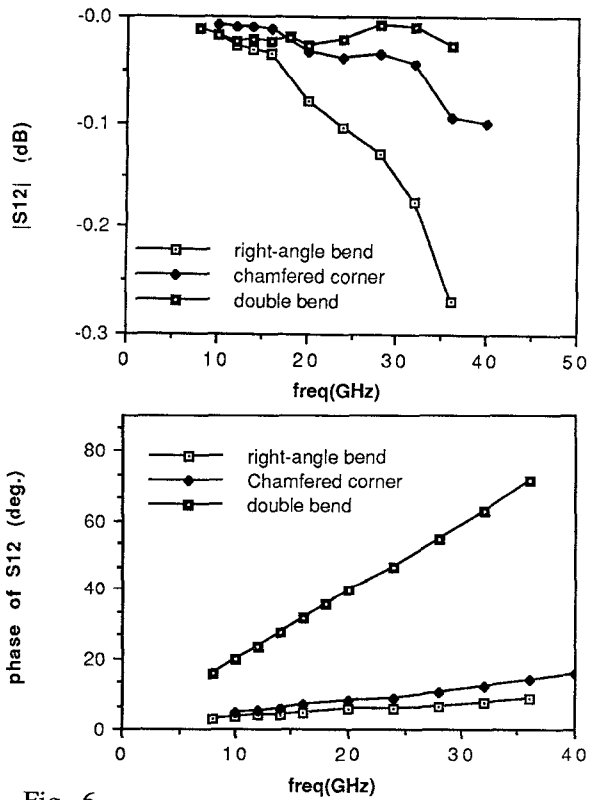


Fig. 6

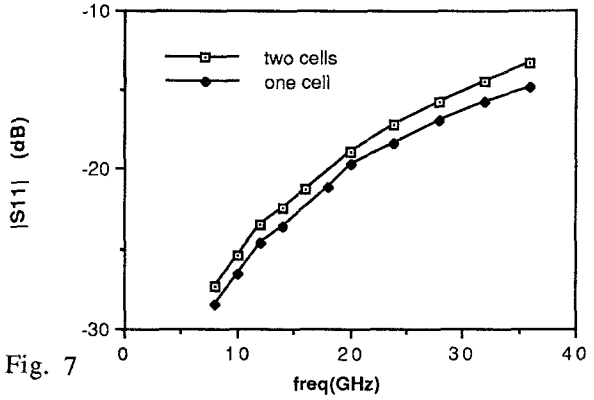


Fig. 7

Figure 7 shows a comparison between the calculated $|S_{11}|$ of the right-angle bend with one cell and two cells in transverse direction. Fast convergence is obtained.

References:

1. D. C. Chang and J. X. Zheng, "Numerical Modelling of Planar Circuit with Pseudo Meshes", URSI Meeting Digest, Boulder, Colorado, Jan. 1990, Page 265.
2. R. Chadha and K. C. Gupta, "Compensation of Discontinuities in Planar Transmission Lines", Trans. Microwave Theory Tech., Vol. M77-30, Number 12, Dec. 1982.
3. Wolf, "CAD Oriented Modelling of Discontinuities in Microwave and Millimeter Wave Transmission Structures", CAD Workshop Digest, Internat. Symp. MTT, New York, May 1988.
4. A. Sabban and K. C. Gupta, "Multiport Network Method for Evaluating Radiation from Discontinuities in Microstrip Circuits", URSI Meeting Digest, Boulder, Colorado, Jan. 1989, Page 66.
5. B. L. Brim and D. C. Chang, "Accelerated Numerical Computation of the Spatial Domain Dyadic Green's Function", URSI Meeting Digest, Boulder, Colorado, Jan. 1987, Page 164.
6. Doris I. Wu and D. C. Chang, "A Modified One-dimensional Method for Solving Microstrip Bend and Discontinuity Problems", URSI Meeting, San Jose, California, June 1989, Page 37.